VTT Technical Research Centre of Finland

Simulation of the Incompressible Viscous Flow around an Endplate Propeller Using a RANSE Solver

Sanchez Caja, Antonio; Sipilä, Tuomas; Pylkkänen, Jaakko

Published in:
Proceedings of the 26th Symposium on Naval Hydrodynamics

Published: 01/09/2006

Document Version
Publisher's final version

26th Symposium on Naval Hydrodynamics
Rome, Italy, 17-22 September 2006

Simulation of the Incompressible Viscous Flow around an Endplate Propeller Using a RANSE Solver

A. Sánchez-Caja, T. P. Sipilä and J.V. Pylkkänen
(VTT Technical Research Center of Finland)

ABSTRACT

Within EU Project LEADING EDGE (LE) several RANS solvers have been applied for predicting the performance and flow patterns around marine propellers. The investigation included three propellers: a conventional, a high skewed and an endplate one. The two first propellers were subject to comparative RANS studies among the LE partners. VTT independently analyzed the third one. A summary of the results for the endplate propeller analysis is presented here. Special emphasis is set on describing the flow over the endplate. The flow is simulated using solver FINFLO. FINFLO is a multi-block cell-centered finite-volume computer code with sliding mesh, moving-grid and free-surface capabilities. Computations are made at model and full scale using the k-ε turbulence model. Relative differences between calculations and experiments are presented for performance coefficients in open water condition at model scale. Good correlation with experiments is obtained in terms of overall forces. The calculated flow patterns over the endplate of the propeller are illustrated for one advance number.

INTRODUCTION

The interest in propellers with endplates comes back to 1976 when G.P. Gómez proposed a propeller (TVF or tip vortex free) with blade outline of Kaplan type and endplates (Gomez, 1976). In the mid-eighties he established a company (SISTEMAR) where he developed an improved version of endplate propellers which was called CLT (Contracted and Loaded Tip). Since then several research groups have become interested in this concept and have studied and/or developed their own version of tip-loaded propellers. The loading at the tip has been introduced in different ways: sometimes using curved propeller tips with a smooth shape transition between blade and plate/fin (Andersen et al., 1992); in other cases introducing short bladelets towards both pressure and suction sides of the propeller blade tip (de Jong et al., 1992). Theoretical studies have been made by Gomez (1976, 1992), Goodman et al. (1980), Klaren et al. (1981), Andersen et al. (1986), Sparenberg et al. (1987), Sánchez-Caja (1988), de Jong et al. (1990) and Dyne (2006) among others.

Endplate propellers are known to offer several advantages for particular marine applications where limitations of propeller diameter and/or strong hull wakes at the propeller location are present and no special reverse-motion properties are required from the propulsor. Since the decade of the 70's, they have been installed in certain type of vessels like Ro-ro vessels, reefers, bulk-carriers, tankers, etc. The idea behind this concept can be explained in several either alternative or complementary ways.

From the standpoint of propeller efficiency, in principle the outer blade sections of a propeller contribute more effectively to the generation of thrust than the inner ones. This results from the fact that the lift they develop is more oriented in the propeller axial direction, i.e. the direction of ship motion. However, the maximum generation of lift, or more specifically the maximum of circulation, cannot be located at the tip since it would result in the generation of strong vorticity (tip vortex) with related energy losses. For conventional optimum propellers the maximum circulation is located at about 70 percent of the propeller radius. Between the location of maximum circulation and the tip, there is a 30

percent of radius to gradually decrease the circulation to zero at the tip avoiding severe vorticity losses. For the case of endplate propellers the span of the endplate is an additional area where the vorticity can be spread. This allows to locate the maximum of circulation closer to the tip as compared to a conventional propeller, and consequently to increase the efficiency.

From the standpoint of propeller vibrations, the longer chord lengths at the propeller tip allow the propeller sections to work in wider sectors of the propeller disk covering simultaneously areas where the changes in local wake can be strong. Additionally the smaller optimum diameter of endplate propellers combined with the availability of longer chords at the tip may locally decrease the loading per square meter at the region more prone to cavitate (i.e. the tip) and consequently in some cases cavitation extension may be reduced. This two-fold effect may result in a reduction of vibrations for a particular application.

Another issue related to the endplates is whether they could develop additional thrust since they work in a similar way as duct sections do in propellers with nozzles. In principle, radial velocities are responsible for the generation of thrust in nozzles, and so do they contribute to the production of thrusting lift for propellers with endplates located towards the suction side of the blades. However, the additional viscous drag over the plates together with the fact that the direction of plate lift is the pitch line at the tip (i.e. not very much oriented to the direction of ship motion) will conceal such effect and the net resultant force on the plate will be a small negative drag for a good design. In fact, some lifting line calculations for optimum distributions of circulation adapted to endplate propellers confirm this conclusion, and show also that the location of the plate either to the suction side or to the pressure side does not significantly affect the overall efficiency of the propeller (Sánchez-Caja, 1988). Only for high propeller loadings does the location of the plate seem to have an influence on efficiency and could the contribution of the endplate result in small positive thrust.

Generally, the design of the endplate for an endplate propeller is difficult task since the shape, actual location and orientation of the endplate should be carefully studied to avoid flow separation phenomena or inadequate plate loading, which would negatively affect the propeller performance. Additionally at full scale the separation patterns over the plate can be significantly reduced as compared to those present at model scale, and this should be accounted for within the design procedure.

From the previous considerations we can conclude that RANS methods are expected to offer valuable assistance in the design process for this type of propulsors where viscous effects play a major role and their proper treatment may be the main issue for a successful design. In the present paper, the RANS equations are solved for an endplate propeller using the FINFLO code initially developed at the Laboratory of Aerodynamics at Helsinki University of Technology (Siikonen, 1990). The flow around blades with endplates is simulated and overall forces from the computations are compared to those obtained from model scale experiments in open water condition. At full scale computations are also conducted and the results are compared to those obtained at model scale in terms of forces and flow patterns.

NUMERICAL METHOD

The flow simulation in FINFLO is based on the solution of the RANS equations by the pseudo-compressibility method. FINFLO solves the RANS equations by a finite volume method. The solution is extended to the wall and is based on approximately factorized time-integration with local time-stepping. The code uses either Roe's flux-difference splitting or Van Leer's flux-vector splitting. A multigrid method is used for the acceleration of convergence. Solutions in coarse grid levels are used as starting point for the calculation in order to accelerate convergence. A detailed description of the numerical method including discretization of the governing equations, solution algorithm, etc. can be found in Sanchez-Caja et al. (1999 and 2000). Chien's low Reynolds number k-ε model was used in the calculation.

GEOMETRY, MESH AND BOUNDARY CONDITIONS

MARIN Propeller Model No. 6613 was selected for the calculations. The model is a right-handed, four-bladed propeller with a diameter of 0.239 m. The hub diameter ratio is 0.329. The expanded area ratio is 0.539 and the skew is moderate. The onset flow for

the calculations corresponds to an advance number of 0.780. The diameter at full scale is 4.300 m. The scale factor is l:18.

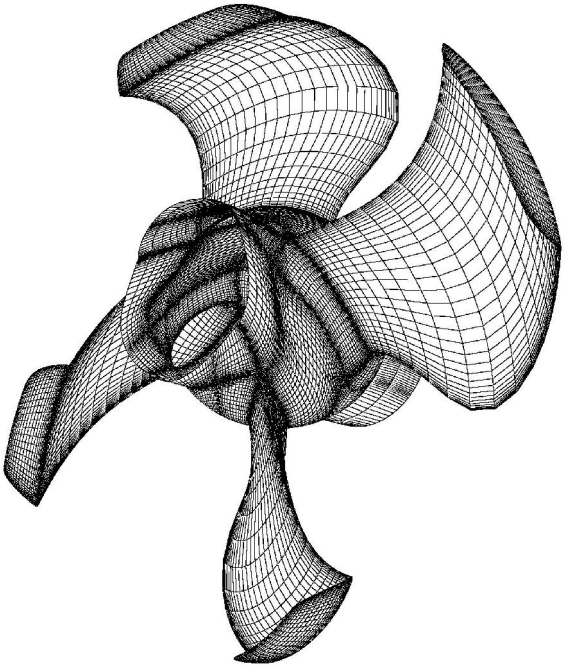

Figure 1a. Grid on the surface of the endplate propeller. Every other line is drawn to facilitate the illustration. Detail of grid construction on the hub. Model scale grid.

Table I. Number of cells in the mesh

Blade surface	Endplate surface	Total Grid Model scale	Total Grid Full scale
12,800	8,960	3,264,000	3,699,200

VTT generated the computational mesh with the IGG grid program and an in-house built program. The model scale grid used in the present calculations consisted of 3,264,000 cells distributed in 11 blocks. The full scale grid was similar, but somewhat larger with 3,699,200 cells. Both grids have the same number of cells on the rotating surfaces. A total amount of 12,800 and 8,960 cells were located on the blade and endplate surfaces, respectively (Table I).

Figure 1a shows an overall view of the computational mesh on the propeller surface for the second level of the grid, i.e. the actual grid has twice as many cells in each grid direction as those shown in the picture. Figure 1b is a cut through the mesh between the blades at model scale. The X-axis is positive downstream. Figure 1c is the model scale grid on a cylindrical surface at a radius of 0.7R.

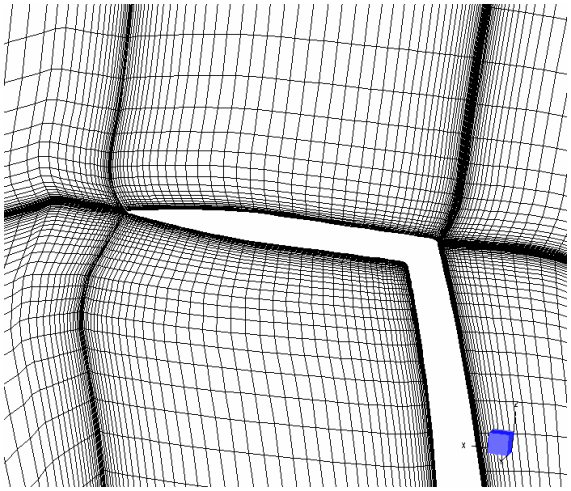

Figure 1b. A cut through the grid between the blades for the endplate propeller. Detail of grid construction on the endplate. Model scale grid.

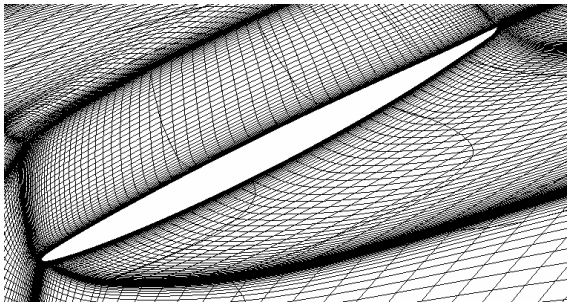

Figure 1c. The grid at a developed cylindrical surface (r=0.7R). Model scale grid.

Two tip vortex areas that will be analyzed in the next sections contained about 40*20 cells in their core for the vortex present at the juncture of blade and endplate, and 13*14 cells for that at the endplate outer tip for the model scale grid. At full scale the grid had about 10*10 cells in both vortex areas.

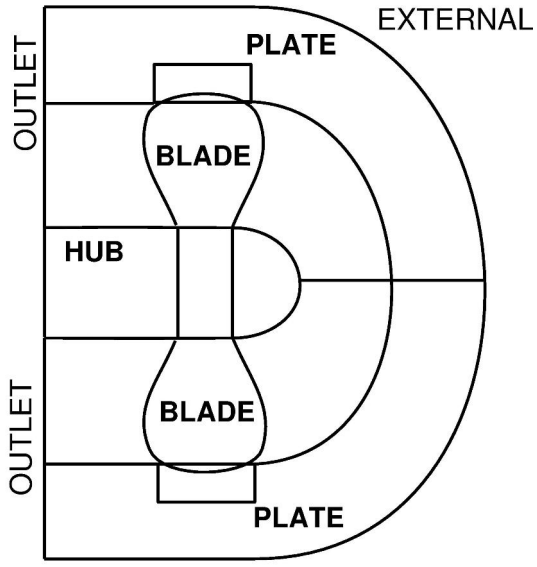

Figure 2a. Grid topology. Axial view.

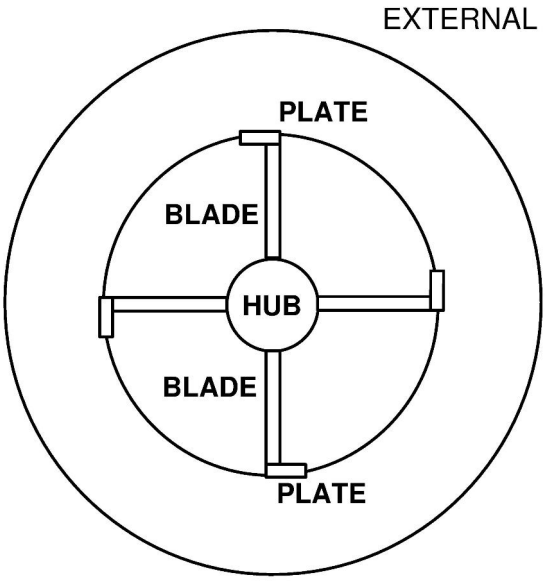

Figure 2b. Grid topology. Transversal view.

Contrary to the conventional and the high skew propeller where O topology was chosen around the blades, for the endplate propeller H-H topology was selected over the propeller blades for its simplicity. C topology was used around the hub, and O topology for the outer domain. Figures 2a and 2b show the topology.

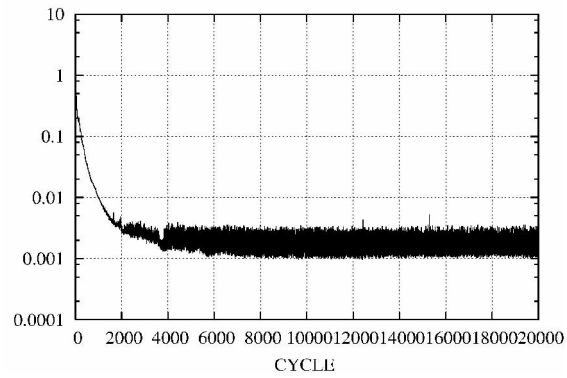

Figure 3a. Convergence history of residuals for x-momentum in the second grid level (coarse grid). Full scale calculation.

The boundary conditions were as follows. The upstream cap of the hub and surfaces of the propeller blades are rotating solid walls with boundary conditions enforcing the velocity field to match the propeller rotational speed. The downstream shaft is also a rotating solid wall. A uniform flow condition is applied to the inlet and peripheral surfaces (external boundary condition). At the computational infinity the boundary conditions are inspired from traditional propeller momentum theory, i.e. uniform flow is applied to the inlet and peripheral surfaces and the streamwise gradients of the flow variables as well as the pressure difference are set to zero at the outlet. Only the portion between two contiguous blades has been used in the computations due to the periodicity of the solution.

CONVERGENCE

The computations were performed on SGI Origin 2000 with 8 processors for the model scale calculation and on Xeon™ with 6 3.06 GHz processors for the full scale one.

In solving the differential equations the multigrid method was applied with two multigrid levels for acceleration of convergence. Also convergence was accelerated by starting the calculation with the solution on a coarse grid, i.e. on that of the previous grid level. Figures 3a and 3b show an example of the

second and the first grid level convergence histories of the x-momentum residuals and drag, respectively for the full scale computation. The second grid level computations were inexpensive (8 times smaller grid) and were continued to 20000 iterations. For the fine grid the changes in drag are minimal after 5000 iterations.

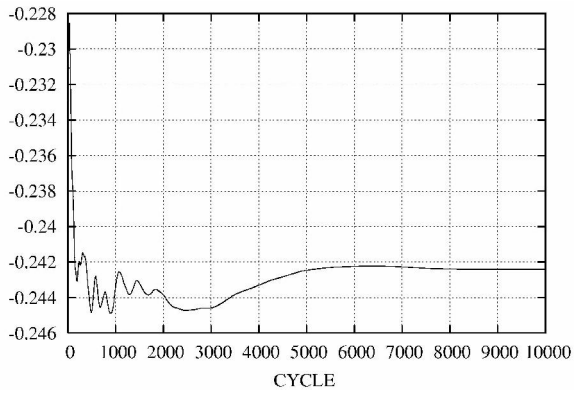

Figure 3b. Convergence history of an overall drag coefficient for the first grid level (fine grid). Full scale calculation.

FORCE ANALYSIS

Table II shows the influence of the grid size on the performance prediction. The first grid level corresponds to a 3.264 million cell grid, the second to 0.408 million cells and the third to a 0.051 million cells. The large size of the original grid allows to have y^+ values of about 5 for the coarsest level, which may be reasonable for boundary layer computation. The grid size seems to affect mainly the torque coefficient (K_Q), which is significantly overpredicted for the coarsest grid. The thrust coefficient (K_T) is not influenced too much by the grid size. The efficiency (η) is underpredicted for coarse grids in smaller proportion than the overprediction of torque mentioned before.

At the first level the differences in calculated thrust and torque coefficients, and efficiency were 1.0, 3.3 and 2.3 percent of the measured values, respectively.

Table III shows the scale effect on thrust, torque and efficiency as percentages of their values at model scale. The increase in thrust is remarkable (9.7 percent). The torque coefficient is less affected by the scale effect. However, the change in torque caused by scaling seems to be higher than that apparent in conventional propellers.

Table II. Percentual differences between experimental and calculated performance coefficients for J=0.78

	Measured	Calculated		
		1st level	2nd level	3rd level
K_T	100.0	101.0	103.2	104.1
K_Q	100.0	103.3	110.2	122.6
η	100.0	97.7	93.7	84.7

Table III. Scale effect on performance coefficients relative to model scale values in percentages for J=0.78. First level grid.

	Calculations	
	Model scale	Full scale
K_T	100.0	109.7
K_Q	100.0	103.6
η	100.0	105.9

Table IV(a). Influence of the plate forces on propeller thrust in percentages of overall thrust for J=0.78

	Calculations	
	Model scale	Full scale
K_{TB}	101.1	100.7
K_{TF}	-1.1	-0.7
K_T	100.0	100.0

Table IV(b). Influence of the plate forces on propeller torque in percentages of overall torque for J=0.78

	Calculations	
	Model scale	Full scale
K_{QB}	95.4	96.5
K_{QF}	4.6	3.5
K_Q	100.0	100.0

Table V(a). Influence of the plate forces on propeller thrust in percentages of model scale *overall thrust for J=0.78*

	Calculations	
	Model scale	Full scale
K_{TB}	101.1	110.5
K_{TE}	-1.1	-0.8
K_T	100.0	109.7

Table V(b). Influence of the plate forces on propeller torque in percentages of model scale *overall torque for J=0.78*

	Calculations	
	Model scale	Full scale
K_{QB}	95.4	99.9
K_{QE}	4.6	3.7
K_Q	100.0	103.6

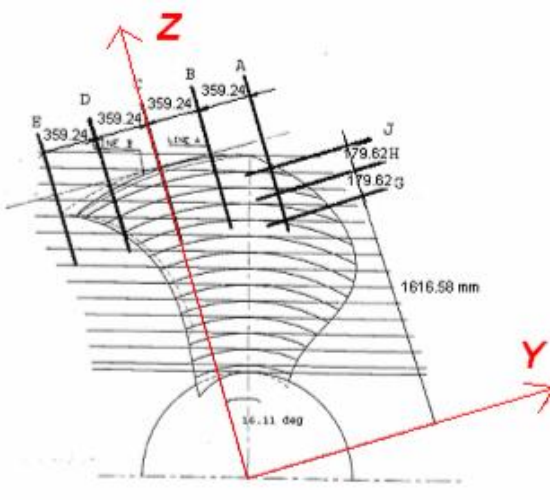

Figure 4. View of the eight reference planes for output analysis.

Table IV(a) shows the contribution of the blade without endplate (K_{TB}) and of the endplate (K_{TE}) to the total thrust coefficient in percentages of the total thrust (K_T). The drag of the plate represents 1.1 percent of the total thrust coefficient at model scale and 0.7 at full scale. Table IV(b) shows the corresponding contributions of torque.

Table V(a) shows the contribution of the blade without endplate (K_{TB}) and of the endplate (K_{TE}) to the total thrust coefficient in percentages of the *model scale* total thrust ($K_{T\text{-model}}$). The full scale drag coefficient of the plate represents 0.8 percent of the total thrust coefficient at model scale. Table V(b) shows the corresponding contributions of torque in percentages of the model scale total torque ($K_{Q\text{-model}}$).

FLOW ANALYSIS

Reference planes

Eight reference planes were specified for analysis. The locations of the reference planes at full scale are given in Figure 4.

Flow visualization

Figures 5a and 5b show the pressure distribution on the pressure side of the blade for the model and full scale calculation, respectively. Figures 6a and 6b show the corresponding distributions for the suction side. The low pressure areas at the leading edge on the suction side are typical for skewed blades and coincide with the location of the leading edge vortex as it proceeds downstream, develops and detaches from the blade at the outer radii.

Figures 7a and 7b show respectively for model and full scale the streamlines and pressure distribution on the suction side of the propeller. The flow separates on the upper side of the endplate at the junction of the main blade and the tip plate as the streamlines detach from the top of the tip plate at a visible angle relative to the pitch line. However, the free vorticity generated at the juncture of endplate does not evolve in the form of tip vortex. The vortex shown later in Figures 11-14 near the juncture is of other nature, i.e. it is a detached vortex produced by the leading edge flow at lower radial stations. Figures 7 illustrate the high three-dimensionality of the flow at the tip. At model scale the limiting streamlines on the upper part of the endplate do not reach the borders at the leading edge and trailing edge, which is indicative of flow separation on both areas (Fig. 7a). At full scale the flow is completely attached (Fig. 7b) on the endplate.

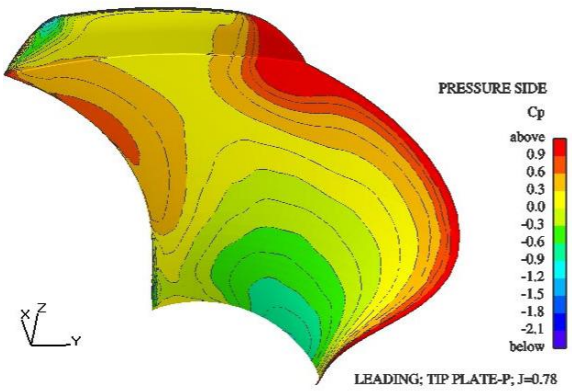

Figure 5a. Pressure distribution on the pressure side of the blade. Model scale calculation.

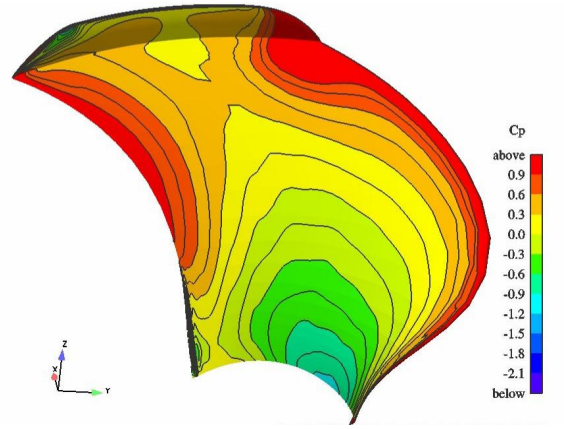

Figure 5b. Pressure distribution on the pressure side of the blade. Full scale calculation.

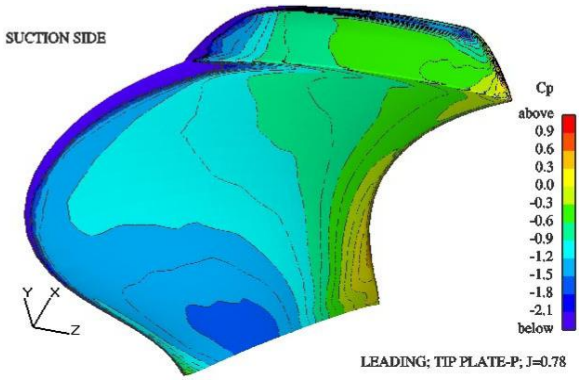

Figure 6a. Pressure distribution on the suction side of the blade. Model scale calculation.

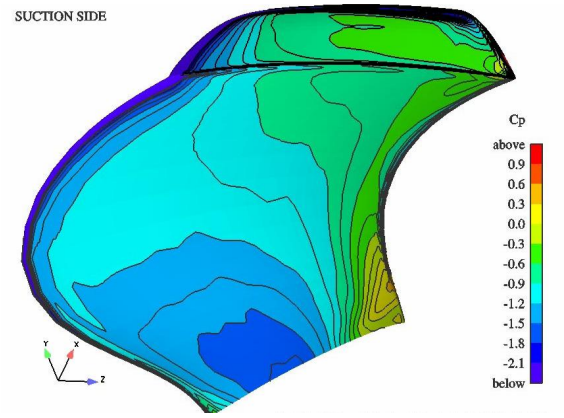

Figure 6b. Pressure distribution on the suction side of the blade. Full scale calculation.

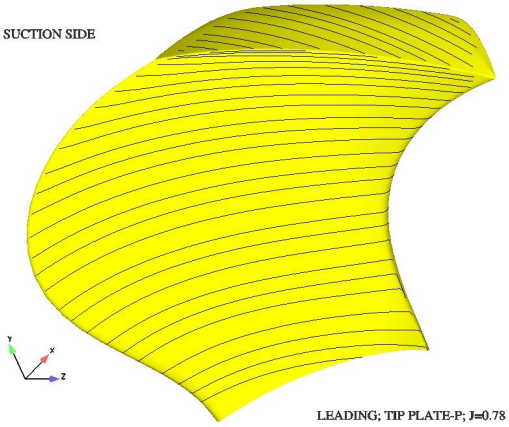

Figure 7a. Streamlines on the suction side of the blade. Model scale calculation.

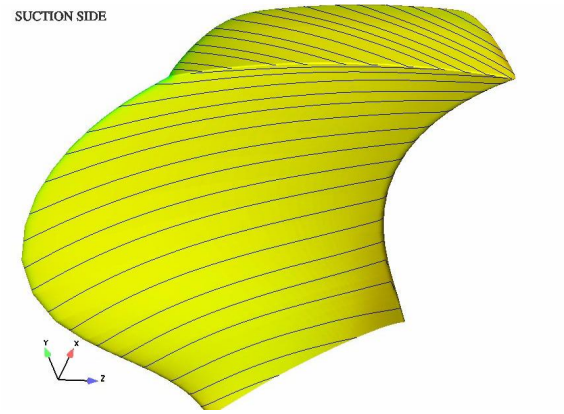

Figure 7b. Streamlines on the suction side of the blade. Full scale calculation.

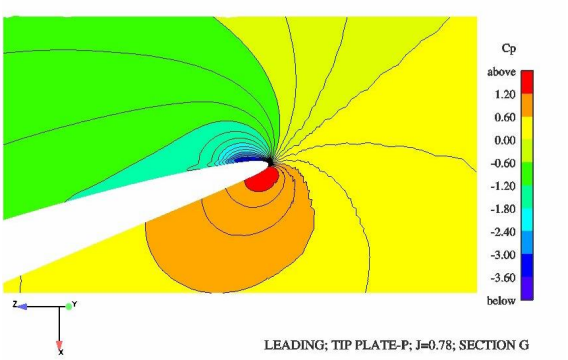

Figure 8a. Pressure distribution on the blade leading edge. Model scale calculation. Reference plane G.

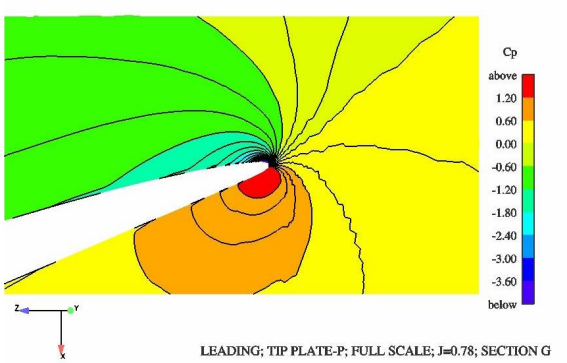

Figure 8b. Pressure distribution on the blade leading edge. Full scale calculation. Reference plane G.

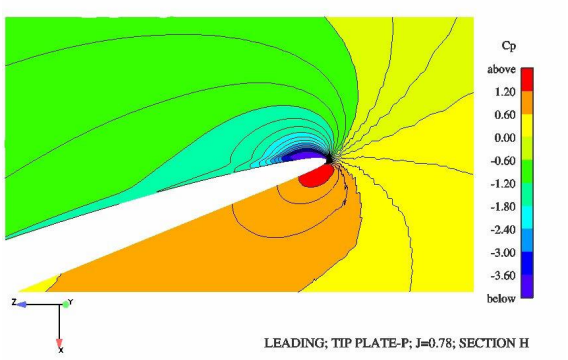

Figure 9a. Pressure distribution on the blade leading edge. Model scale calculation. Reference plane H.

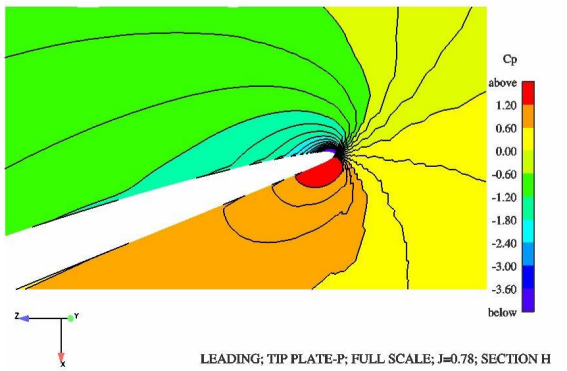

Figure 9b. Pressure distribution on the blade leading edge. Full scale calculation. Reference plane H.

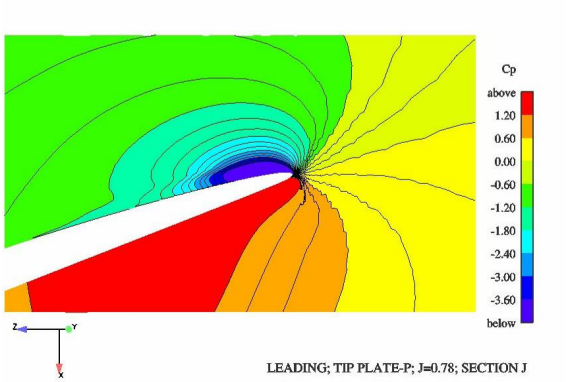

Figure 10a. Pressure distribution on the blade leading edge. Model scale calculation. Reference plane J.

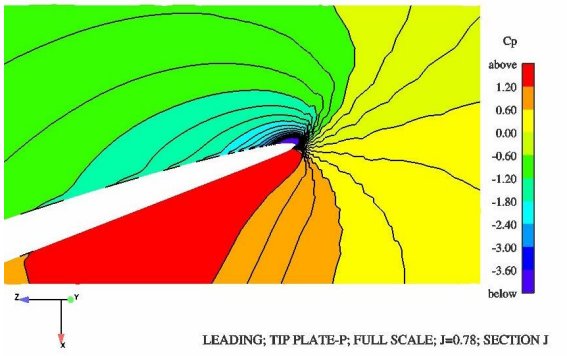

Figure 10b. Pressure distribution on the blade leading edge. Full scale calculation. Reference plane J.

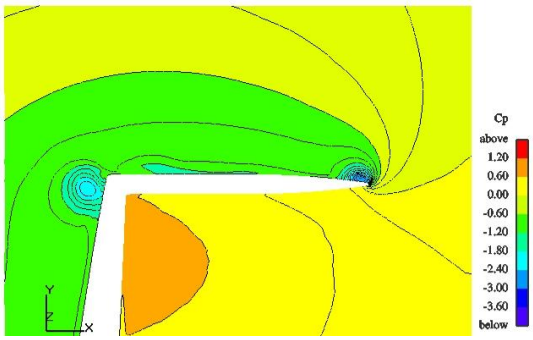

Figure 11a. Pressure distribution on the endplate. Model scale calculation. Reference plane B.

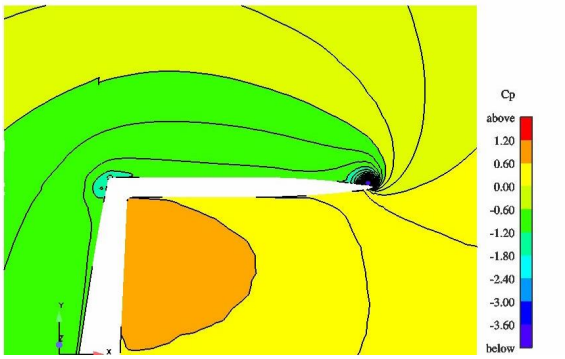

Figure 11b. Pressure distribution on the endplate. Full scale calculation. Reference plane B.

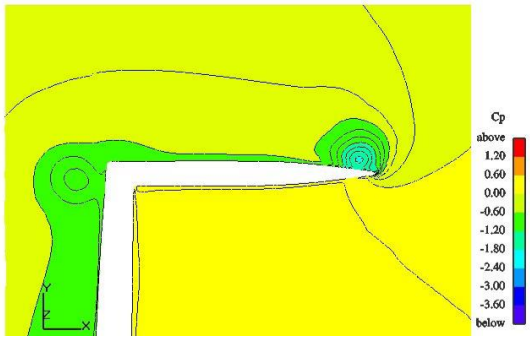

Figure 12a. Pressure distribution on the endplate. Model scale calculation. Reference plane C.

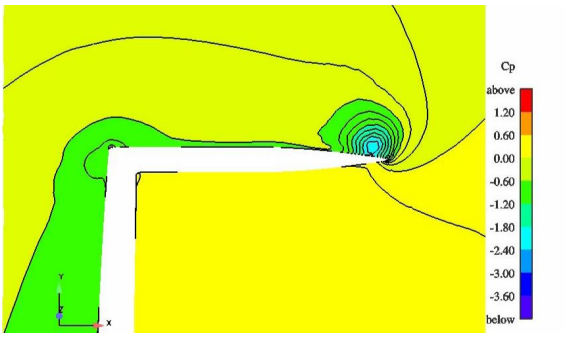

Figure 12b. Pressure distribution on the endplate. Full scale calculation. Reference plane C.

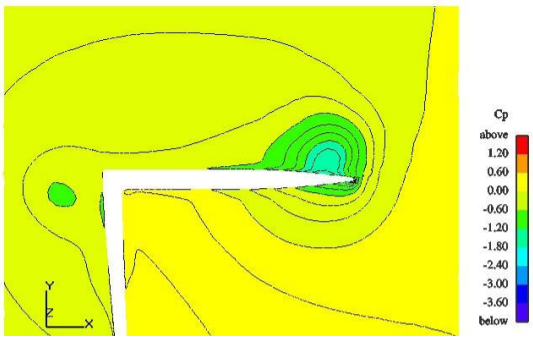

Figure 13a. Pressure distribution on the endplate. Model scale calculation. Reference plane D.

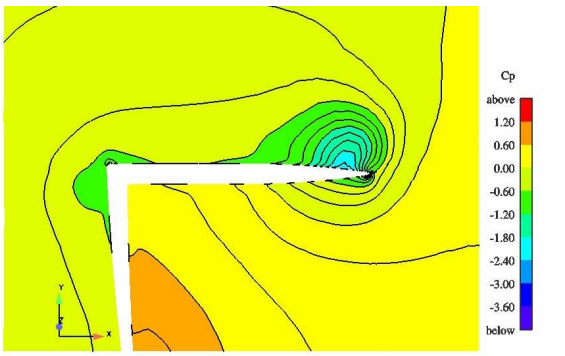

Figure 13b. Pressure distribution on the endplate. Full scale calculation. Reference plane D.

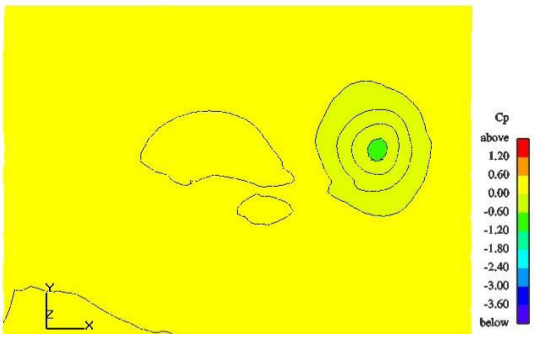

Figure 14a. Pressure distribution on the endplate wake. Model scale calculation. Reference plane E.

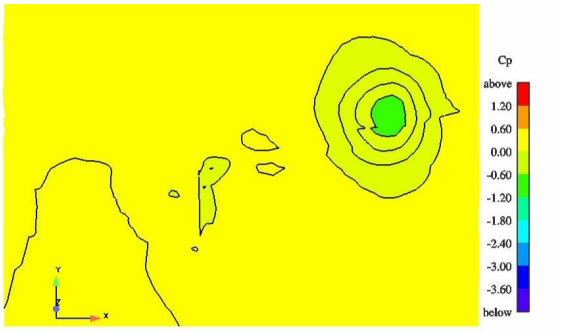

Figure 14b. Pressure distribution on the endplate wake . Full scale calculation. Reference plane E.

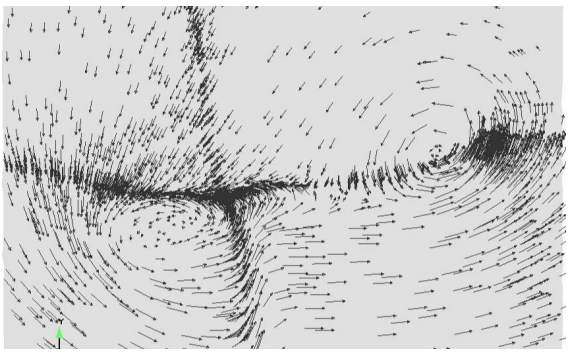

Figure 14c. In-plane velocity vectors on the endplate wake. Model scale calculation. Reference plane E.

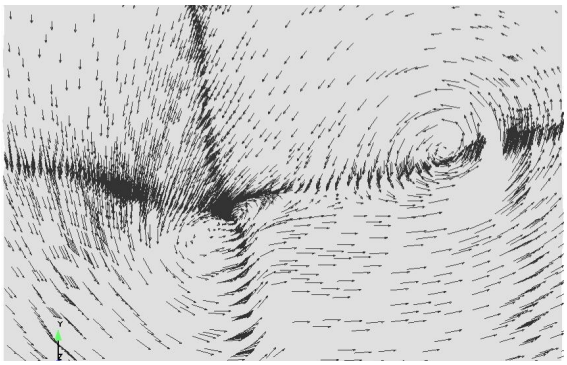

Figure 14d. In-plane velocity vectors on the endplate wake. Full scale calculation. Reference plane E.

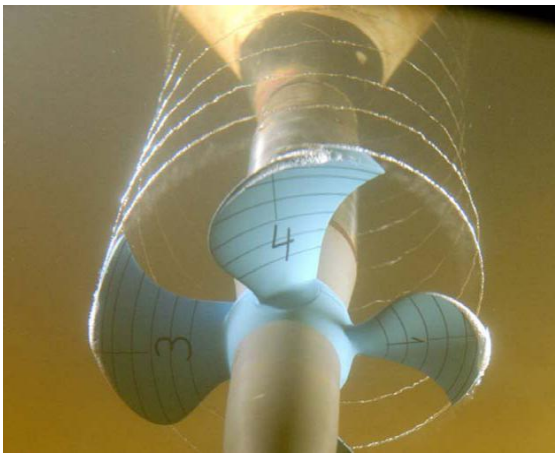

Figure 15a. Developed sheet cavity on the blade

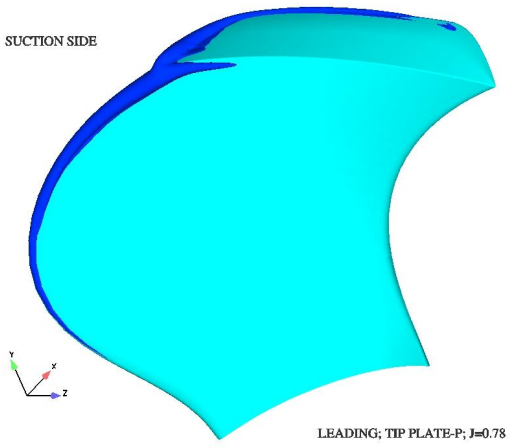

Figure 15b. Low pressure isosurfaces on suction side.

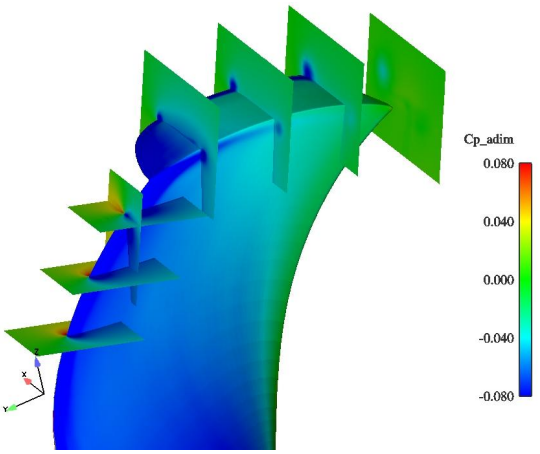

Figure 16. Artistic view of the evolution of pressure on the blade leading edge and endplate outer border. Model scale.

Figures 8a and 8b show the pressure distribution on the blade leading edge for the model and full scale calculation, respectively at reference plane G. The low pressure area in the pictures is identified with the leading edge vortex. The evolution of the leading edge vortex can be followed in Figures 9a and 9b on plane H, and 10a and 10b on plane J. The leading edge vortex is clearly stronger at model scale than at full scale.

Figures 11a and 11b show respectively for model and full scale simulation the pressure distribution on the endplate on reference plane B. The leading edge vortex is detaching from the blade at the tip corner at model scale. At full scale the vortex seems to be still attached to the blade corner and is weaker. Another vortex at the endplate tip is being generated on the right side of the pictures. The vortex is somewhat stronger at full scale.

The evolution of the vortices is seen in Figures 12a and 12b for reference plane C, in Figures 13a and 13b for plane D, and in Figures 14a and 14b for plane E. Figures 14c and 14d illustrate the in-plane velocity vectors on the endplate wake. From the figures the leading edge vortex fades away faster at full scale than at model scale. By contrast, the endplate tip vortex is stronger at full scale.

Cavitation inception and developed cavitation tests were conducted for this propeller. Figure 15a shows the results of developed cavitation tests. Figure 15b shows some low pressure isosurfaces for comparison at model scale. The low pressure areas seem to qualitatively agree. The calculation presented in this paper was made without the cavitation model activated.

Figure 16 illustrates the evolution of low pressure areas at model scale.

DISCUSSION

The results presented in this report show how RANS solver FINFLO has been used to simulate the main features of the flow around an endplate propeller. In particular the calculations show how the endplate succeeds in preventing the generation of tip vortex at the blade tip. Instead a weak vortex appears at the endplate outer edge. The development of leading edge vortices typical in skewed blades and of other tip vortices has been illustrated. There are open questions concerning scale effects for which it would be desirable to have validation data at full scale; in particular the attached nature of the leading edge vortex at full scale, and the slightly stronger intensity of the vortex generated at the endplate outer edge at full scale.

Even though flow regimes in model scale calculations and experiments may differ to some extent due to deficiencies in turbulence modeling reasonable agreement in overall forces for propeller flows has been obtained in many propeller studies as was the case for the propeller subject to this investigation. Grids with high density of cells that accurately model the propeller geometry are essential for obtaining grid independent solutions.

RANS calculations have shown a large scale effect on thrust coefficient for this particular endplate propeller (almost 10 percent), much larger than that found for conventional propellers. Usually cavitation tests are made in such a way that a dynamic similarity prevails over the kinematic one, i.e. K_T at full scale is sought in model scale tests. For conventional propellers where scale effects on thrust are not so acute, one can expect that the kinematic similarity (J identity) is more or less fulfilled in tests with K_T identity. However, for endplate propellers the kinematic similarity may be questioned if cavitation tests are conducted in the traditional way. Aiming at a K_Q or J identity in the tests would be a better choice in this respect.

High efficiency and large cavitation-free operation are usually conflicting requirements for propeller flows. In principle the availability of large chord lengths at the tip for endplate propellers allows to decrease the loading per unit area, which is beneficial from the standpoint of cavitation. However, for extreme conditions the high velocities at the propeller tips make it always difficult to control cavitation. Generally, endplates located towards the blade suction side should perform better from efficiency standpoint. However, from cavitation standpoint it would be advisable to locate them on the pressure side. In fact, lifting line theory can be utilized to illustrate that the impact of 'pressure side' endplates on efficiency is not expected to be significant. In spite of all, the flow over the endplate is highly three-dimensional and it is not clear from simple theories what is the best location for the endplates.

For moderately loaded propellers endplates on their own have limited capability of producing thrust. This is a consequence of the fact that the plate lift is directed almost radially with only a small component in the direction of the pitch line at the tip. Additionally the 'small component' is not very much oriented to the direction of ship motion due to the small hydrodynamic pitch angle at the tip. Therefore, the thrust produced by the plate is marginal compared to that developed by the neighboring blade sections and no drastic changes of performance due to the endplate location can be expected due to lift developed by the plate. In contrast the drag force on the plate is pointing close to the circumferential (tangential) direction, i.e. the direction of torque production. Therefore excessive drag due for example to flow separation for bad plate design would result in a severe penalty on efficiency.

Remarkable increases in efficiency are expected for propellers designed for high loadings. However, such efficiency gains would depend on the possibility to reach ideal conditions of undetached flow, free-cavitation operation, etc. For such conditions models with a proper treatment of viscosity effects (for example RANS based ones) would be more appropriate as prediction tools. Higher performance for heavily loaded condition is in line with the model experiments presented in Gent et al. (1992) where large improvements in efficiency were shown at low advance numbers for propellers with double plates.

CONCLUSIONS

The incompressible viscous flow around an endplate propeller has been simulated by solving the RANS equations with the k-ε turbulence model at both model and full scale. The FINFLO code was used for the calculations. The grids contained over 3 million cells. Good correlation with model scale experiments is obtained in terms of force coefficients. The thrust coefficient has been calculated with 1 percent error for an advance number of 0.78. The torque coefficient differs from measurements by 3.3 percent. Important features of the flow, like the leading edge vortex typical of skewed blades and the vortex at the outer region of the endplate were identified. The contribution of endplates and blades to the total propeller forces is illustrated. Some considerations on cavitation and efficiency are made. The results of the computations show that RANS solvers are a valuable tool for assisting the propeller designer.

ACKNOWLEDGEMENTS

This work has been made within the European Union LEADING EDGE project. The authors wish to thank the partners in the LEADING EDGE consortium for allowing this publication. Special thanks are given to NAVANTIA for providing the geometry subject to investigation.

REFERENCES

Andersen, S.V. & Andersen, P. Hydrodynamic "Design of Propellers with Unconventional Geometry," the Danish Center for Applied Mathematics and Mechanics, Report No. 320, February 1986.

Andersen, P. & Schwanecke, H. "Design and Model Tests of Tip Fin Propellers," The Royal Institution of Naval Architects, Vol 134, April 1992.

Dyne, G. On the Principles of Propellers with Endplates, RINA Transactions- International Journal of Maritime Engineering (IJME), Vol 147, 2005, Part A3.

van Gent, W., Falcão de Campos, J.A.C. & de Jong, K., “Model Test Results of an Optimum Propeller with Endplates and some Practical Aspects of Application”, MARIN Jubilee Meeting, Wageningen, May 1992.

Gómez, G.P. “Una Innovación en el Proyecto de Hélices”, Ingeniería Naval, October 1976.

Gómez, G.P. & González-Adalid, J., “Tip Loaded Propellers (CLT)- Justification of their Advantages over Conventional Propellers Using the New Momentum Theory”, SNAME 50th Anniversary, 1942-1992.

Goodman, T.R. & Breslin, J.P., “Feasibility Study of the Effectiveness of Tip Sails on Propeller Performance”, Stevens Institute of Technology, Report MA-RD 94081006, September 1980.

de Jong, K. & Sparenberg, J.A., “On the Influence of Choice of Generator Lines on the Optimum Efficiency of Screw Propellers”, Journal of Ship Research, Vol. 23, No. 2, June 1990, pp. 79-91.

de Jong, K., Sparenberg, J.A., Falcão de Campos, J.A.C. & van Gent, W., “Model Testing of an Optimally Designed Propeller with Two-Sided Shifted End Plates on the Blades”, 19th Symposium on Naval Hydrodynamics, Seoul, August 1992.

Klaren, L. & Sparenberg, J.A., “On the Optimum Screw Propeller with Endplates”, Journal of Ship Research, Vol. 25, No. 4, December 1981, pp. 252-263.

Sánchez-Caja, A. “An Approach to the Design of a Tip Loaded Propeller.” Spring-term paper of the course ‘Hydrofoils and Propellers’, MIT, May 1988.

Sánchez-Caja, A., Rautaheimo, P., Salminen, E., & Siikonen, T., "Computation of the Incompressible Viscous Flow around a Tractor Thruster Using a Sliding Mesh Technique," 7th International Conference in Numerical Ship Hydrodynamics, Nantes (France), 1999.

Sánchez-Caja, A., Rautaheimo, P. and Siikonen, T., "Simulation of Incompressible Viscous Flow Around a Ducted Propeller Using a RANS Equation Solver," 23rd Symposium on Naval Hydrodynamics, Val de Reuil (France), 2000.

Siikonen, T., Hoffren, J., and Laine, S., "A Multigrid LU Factorisation Scheme for the Thin-Layer Navier-Stockes Equations," Proceedings of the 17th ICAS Congress, pp. 2023-2034, Stockholm, Sept. 1990. ICAS Paper 90-6.10.3.

Sparenberg, J.A. & de Vries, J., “An Optimum Screw Propeller with Endplates”, International Shipbuilding Progress, Vol. 34, No. 395, July 1987.